ASSESSMENT OF DEEP LEARNING ALGORITHMS FOR FAULT DIAGNOSIS IN SOLAR THERMAL SYSTEMS

Camila Correa-Jullian[1], José Miguel Cardemil[1], Enrique López Droguett[1], Masoud Behzad[2,1]

[1] Mechanical Engineering Department, Universidad de Chile, Santiago (Chile)

[2]Industrial Engineering School, Faculty of Engineering, Universidad de Valparaíso, Valparaíso (Chile)

Abstract

Solar hot water (SHW) systems are viable and sustainable devices for hot water domestic and industrial energy needs. Nevertheless, the efficient operation of these systems can be compromised if the necessary maintenance measures are not implemented. Degradation of components and malfunction in SHW systems may undergo unnoticed when coupled to traditional auxiliary energy sources. Detailed and continuous monitoring to counter this, however, elevates the overall cost of the system and thus, other methods have been explored for performance assessment and fault detection. Data-driven techniques became popular as Prognosis and Health Management approaches in mechanical components for detection, diagnostics and prognostics of complex systems. In this article, Deep Learning algorithms, such as ANN, RNN and LSTM, are analyzed as alternatives for performance prediction and anomalous behavior detection in a solar hot water system. TRNSYS simulation software is used to generate synthetic operation data for the system for nominal operational and fault-induced conditions. Similar results were obtained for the temperature predictions, with the LSTM models obtaining a lowest combined RMSE of 1.27°C, MAE of 0.55°C and variance 0.52 $°C^2$, as well as the lowest relative prediction errors of 3.45%, indicating a more reliable performance. Using this model, the prediction-based anomaly detection was tested under different meteorological conditions, where overheating and heat underproduction anomalies were detected with a mean accuracy of 85% and 82%, respectively.

Keywords: Solar hot water systems, performance forecast, anomaly detection, Deep Learning.

1. Introduction

Improving the performance and reliability of renewable energy systems, aiming to reduce the associated investment and operational costs, is a high priority for scientists and engineers since it represents the biggest entry barrier to a market currently dominated by fossil-fuel based energy sources (IRENA, 2018). Fault detection and diagnostics can be achieved through various techniques, from simulation and model-based approaches to data-driven methods. During the past decade, several Machine Learning (ML) applications have been explored in Prognosis and Health Management (PHM) focused on increasing the availability and performance of complex systems, as well as assisting maintenance and other decision-making analysis (Niu, 2017). Based on the available information, a ML algorithm can learn from the data, extracting abstract relationships within the studied variables to classify or predict future values. Within these, the growing success and popularity of Deep Learning (DL) techniques for reliability and maintenance in mechanical systems have led, for instance, to successful fault detection in rotary machinery (Janssens et al., 2016) and the estimation of Remaining Useful Life (RUL) in lithium-ion batteries (Lui et al., 2017), among others.

Solar hot water (SHW) systems are commercially mature applications of solar thermal technologies for domestic and low temperature industrial uses. These are frequently coupled to conventional electrically-driven or fossil-fueled back-up systems, as well as thermal storage, which extend the availability of thermal energy limited by the solar radiation's daily profile. Thus, failures or anomalous behavior may not be visible in SHW systems, as the auxiliary sources supply the required energy to fulfill the nominal heat load. Therefore, component failure may go unnoticed since nominal periodical maintenance procedures are not complex enough to take into account degradation issues and replacement needs in specific components. For this reason, frequent inspection and monitoring are important factors in extending the useful life of SHW systems, as well as reducing the energy consumption of conventional heat sources (de Keizer et al., 2013). In this context, performance prediction is also a fundamental tool to assess the state of health of the system and assisting in maintenance scheduling tasks.

In previous literature, the task of performance prediction in solar thermal systems has been addressed with ML

Selection and/or peer review under responsibility of Scientific Committee
doi:10.18086/swc.2019.08.03 Available at http://proceedings.ises.org

algorithms. A thorough review was presented by Ghritlahre and Prasad, referencing over 30 papers regarding the use of different variants of Artificial Neural Networks (ANN) (Ghritlahre and Prasad, 2018). Performance prediction and efficiency analysis under different meteorological conditions are studied in SHW systems, solar assisted heat pumps and thermal storage systems with different neural network models such as Multi-Layered Perceptron (MLP), Radial Basis Functions (RBF) and Adaptive Network-Based Fuzzy Inference System (ANFIS). Fault detection has also been investigated by applying ANN in thermal systems. Kalogirou et al. proposed a fault diagnosis system in which the monitored data is compared to the predicted values, allowing to identify faults in solar collectors with outstanding results (Kalogirou et al., 2008). However, specialized DL architectures, developed for specific tasks, have not yet been tested in SHW systems. For instance, the advantages of implementing solutions based on Recurrent Neural Networks (RNN) for timeseries replication and analysis of temporal relationships, as well as Long Short-Term Memory (LSTM-RNN) implemented for analyzing long-term temporal dependencies have not been thoroughly analyzed in SHW systems (Lipton et al., 2015).

A comparative study of LSTM neural networks in forecasting day-ahead global horizontal irradiance with satellite data was presented in 2018 (Srivastava and Lessmann, 2018). The authors highlight that shallow ML algorithms (Support Vector Machine (SVM), Random Forest, among others) and standard ANN (Feed-Forward Neural Networks (FFNN), RBF, MLP) have been frequently used for radiation forecast, but at the time, no specialized models such as LSTM had been explored for this purpose. This work aimed to obtain an accurate forecast for photovoltaic (PV) based energy plants, since PV power production, stability, and storage dimensioning is strongly influenced by instantaneous meteorological conditions. Predictive features are a critical issue for the electrical grid management and for smart-grid applications: planning, storage system sizing and market participation of variable renewable energy sources (Leva et al., 2017). However, as mentioned, applications of these architectures are scarce in solar thermal systems. Even though thermal systems present a natural inertia which generally reduces the need for high accuracy and precision for temperature predictions, time series-focused algorithms such as RNN and LSTM may lead to better and more precise forecasts than the previous ANN results.

In this work, ANN, RNN and LSTM architectures are analyzed for temperature prediction in a SHW system; and compared under similar conditions to highlight their strengths and shortcomings. Their accuracy and precision are compared for the prediction of future instantaneous values, as well as for short sequences based on the RMSE and MAE scores obtained. The methodology and results of this analysis is thoroughly detailed in (Correa-Jullian et al., 2019). The trained models are used in a further application for detection of anomalous behavior within the system, allowing an early identification of heat underproduction or overheating conditions based on the obtained predictions. By comparing the prediction errors of the model produced when using nominal and fault-induced data, an error-based threshold is determined to classify the health state of the system. Three cases with induced faults are studied under different meteorological conditions. The accuracy, precision, recall, F-1 and specificity scores are reported for this anomalous scenario. Aiming to apply the algorithms to an actual system, the solar-assisted heating loop located at the University of Chile is used as a case of study. Synthetic data is generated in TRNSYS under nominal and anomaly-induced conditions as suggested in (Kalogirou et al., 2008; Souliotis et al., 2009). For building and validating the TRNSYS simulation, the nominal data from the manufacturer was employed, introducing design temperatures, equipment sizes and capacities and the control scheme, of each subsystem.

The following sections of this article are organized as follows. Section 2 briefly describes the configuration of the SHW system, its components, and operation logic. Section 3 presents the methodology used for data recollection and the Deep Learning framework for temperature sequence prediction. Results regarding both temperature prediction and anomaly detection are discussed in Section 4. Finally, Section 5 concludes and highlights the future challenges for the proposed anomaly detection framework.

2. SHW System Description

The SHW system analyzed herein is currently installed at Universidad de Chile, located in Santiago, Chile; and serves as a heat source for supplying hot water to showers, among other sanitary hot water needs. A schematic representation of the system is shown in Fig. 1, where the red and blue lines represent hot and cold-water flows,

respectively. The nominal daily demand is estimated as 24,000 L at 40°C for 12 hours and is provided by two separate heating circuits. The preheating section consists on the SHW system, excess heat from heat-recovery chiller and two intermediate 4 m^3 storage tanks (Pre-Heat Tank 1-2) designed to store water at 30-40°C throughout the year. The storage tanks also receive the returning hot water not dispatched to the system. Subsequently, when hot water is required, both tanks deliver the demand to the heating circuit, where heat pumps complements the heat load to reach 60°C and later stored in four final storage tanks (Hot Tank 1-4). These circuits are connected to the mains water distribution system, used to regulate output temperature and as make-up water in the preheating section. Temperature and operation status are monitored in the SHW system, taking into consideration the tanks, heat-recovery chiller and heat pumps, as well as the heat exchangers and centrifugal pumps. Hitek Solar NSC 58-30 heat-pipe collectors are considered, as well as a Thermocold CWC Prozone 1320 Z C heat-recovery chiller. Table 1 presents the Incidence Angle Modifiers (IAM) reported by the solar collector manufacturer for transverse θ_T and longitudinal θ_L incidence angles. Relevant thermal properties of the heat-pipe collectors used in this installation are detailed in Table 2.

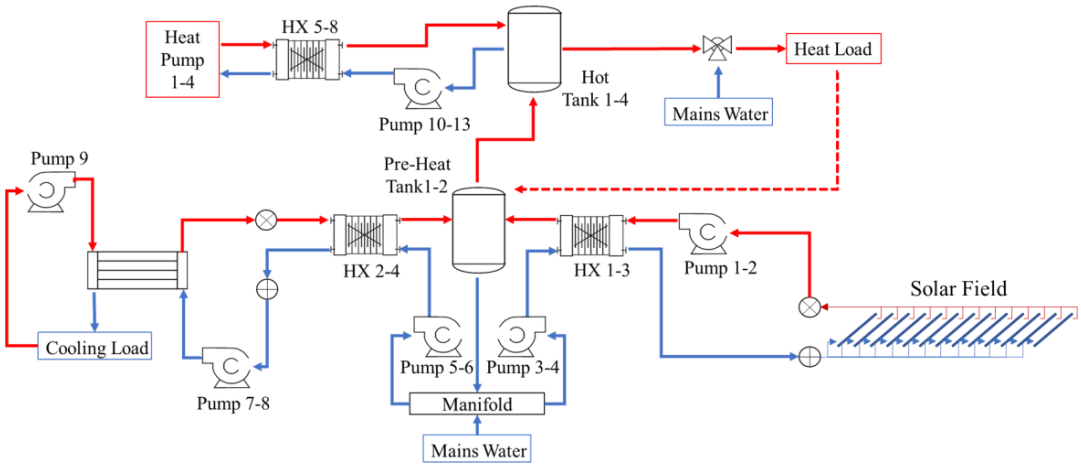

Fig. 1: Schematic process flow diagram of the SHW system.

Tab. 1: Incidence Angle Modifiers values for Hitek Solar NSC model.

IAM Values	*10°*	*20°*	*30°*	*40°*	*50°*	*60°*	*70°*
$K_\theta(\theta_T)$	1.010	1.019	1.056	1.151	1.452	1.462	1.261
$K_\theta(\theta_L)$	0.999	0.994	1.018	0.974	0.952	0.913	0.833

Tab. 2: Thermal capacities of Hitek Solar NSC model.

Parameter	*Value*
$\boldsymbol{\eta_0}$	0.618
$\boldsymbol{a_{1a}}$ $[\boldsymbol{W/m^2K}]$	1.377
$\boldsymbol{a_{2a}}$ $[\boldsymbol{W/m^2K^2}]$	0.018
Effective Thermal Capacity $[\boldsymbol{kJ/m^2K}]$	5.684

3. Methodology

The purpose of the Deep Learning-based framework is to predict future values of the solar collector's outlet temperature based on the generated data from the TRNSYS simulation. In this section, a brief description of the simulation approach in TRNSYS software and the methodology to design the prediction framework is presented. Data recollection is assessed in Section 3.1, including the generation of anomalous temperature profiles. Design decisions regarding the DL models, the training process are detailed in Section 3.2

3.1 Data recollection

Technical data and nominal operating conditions are used as inputs to construct a TRNSYS deck (Klein, 2018), as well as meteorological data from a complete measuring station located close to the solar field. This meteorological station includes measurements of solar radiation (Global, Beam and Diffuse components), ambient temperature, wind speed and wind direction. The following simplifications were considered in the simulation:

- Mains water temperature is estimated based on numeric correlations presented in (Burch and Christensen, 2007).
- Heat pumps are modelled as auxiliary water heaters with the same nominal heating capacities. It must be noted that the temperature setpoint of the four heating water tanks is 60°C to control Legionella growth.
- Nominal conditions are kept constant for returning flows to the heat-recovery chiller which have not been simulated. These returning flows enter the evaporator at 12.7°C and the returning temperature from the secondary heat load at 44.5°C.
- The temperature control systems are simplified as the following:
  - If the temperature registered at the outlet of the solar collector field is higher than the average pre-heating tank temperatures, Pumps 1-2 are activated.
  - Mixing valves are activated if the outlet temperature of the heat tanks is higher than 45°C, in which case mains water is introduced before being dispatched.
- The system operates for 14 hours on weekdays, between 7 AM and 9 PM. During weekends the operation hours are reduced to 11, from 8 AM to 7 PM.
- As no real-time measurements of the hot water demand profile were available, a weekly profile was drawn from estimations of user experience and the design conditions.

Although the model is not experimentally validated due to technical difficulties in the installed system, a comparison between the main temperatures obtained with the simulation and the design temperatures is presented in Table 3. Here, the overall difference accounts temperatures 19.5% higher in the simulation. This is an average difference of 7.7 °C, mainly caused by the higher participation of the solar field. In addition to that, TRNSYS has been applied and validated in different solar thermal studies, such as pool heating, hot water storage tanks, and both flat plate and evacuated tube solar collectors (Ayompe et al., 2011; Kalogirou et al., 2019; Ruiz and Martínez, 2010). Thus, the thermal behavior of the system estimated by TRNSYS constitutes an acceptable approach to explore the DL techniques for performance prediction. The simulation is carried out considering actual radiation data from April 7th to September 22nd, 2018. Resulting temperatures are monitored and extracted at sampling frequency of a minute.

Tab. 3: Comparison of design and simulated temperatures in the SHW system.

Temperature °C	Design	Simulated	Difference
Pre-Heat Tank	35.0	45.2	29.3%
HR Ch. Outlet	50.0	54.5	9.0%
Solar Inlet	37.0	45.0	21.7%
Solar Outlet	45.0	53.2	18.2%
		Average	19.5%

Additionally, anomalous scenarios regarding pump failure and solar collector degradation were simulated, inducing overheating or unexpected reduced heat production, represented as faulty water-draw forcing function and the reduction of incident radiation, respectively. Overheating may be caused by low hot water demand or pump failure. This is mainly due to the logic with which the control system activates the circulation pumps connecting the solar field and the heat exchangers, as well as the lack of other heat-dampening methods to prevent this behavior and reduce the heat delivered. From operational experience, the biggest issues arise from overheating due to lower demand profiles than expected, especially during the summer season. On the other hand, heat underproduction may be associated with unexpected meteorological conditions, degradation, or failure in one or more of its components (de Keizer et al., 2011).

Special interest is devoted to monitoring the solar field outlet temperature, since the traditional sources (heat-

recovery chiller and heat pumps) mask the effect of the anomalous behavior and possible damages in the SHW system. The effect of the anomalous water-draw profiles and the reduction of the collector's efficiency on the outlet temperature of the solar field are shown in Fig. 2. These plots show the difference between healthy and anomalous temperature values caused by the induced fault. Fluctuations in the system with a cycle life shorter than an hour and lower magnitudes cannot be categorically defined as anomalous, since might be explained by the natural variation of the incoming solar radiation.

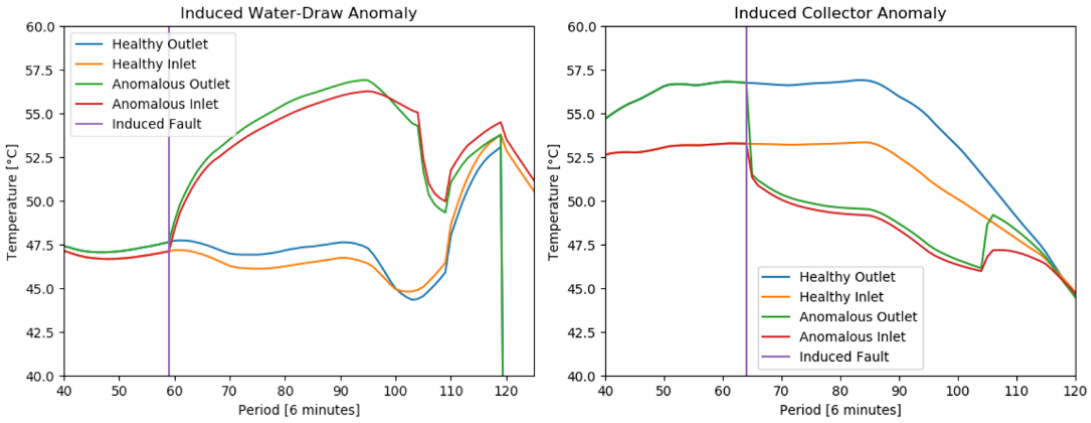

Fig. 2: Anomalous temperature profiles for (a) water-draw anomaly and (b) collector operation anomaly.

3.2 Deep Learning Framework

The prediction of future values from historic operational fault-free data is explored by using DL algorithms. As mentioned, ANN has been frequently used for performance prediction in many different systems. A trained model can extract abstract relationships within the data, interpreting new samples and subsequently replicating the learnt behavior. Model's performance depends on the architecture, the nature of the data, the selected hyperparameters and the training process, which is stochastic in nature.

The basic representation of a single-layered ANN is presented in Fig. 3 (a), in which the output value y is calculated by applying a non-linear transfer function σ to a weighted sum of the input data X. In multiple-layered ANN or Deep Neural Network (DNN), a series of weight matrices (W) and bias (b) vectors represent the transitions between the layers, as shown in eq. 1, in which the input data is the output value from the previous layer (eq. 2). For regression tasks, the final output layer applies a linear function to yield the predicted future value of a time-series.

$$y = \sigma(W^t X + b) \qquad \text{(eq. 1)}$$

$$h_i = \sigma(W_i^t h_{i-1} + b_i) \qquad \text{(eq. 2)}$$

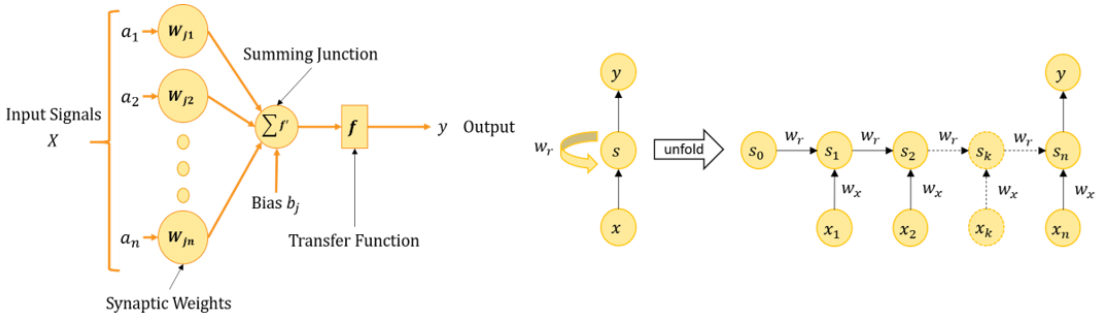

Fig. 3: Basic structure of (a) MLP or ANN (b) Unfolded RNN.

In the case of Supervised Learning methods for regression tasks, the training of the ANN model consists on the adjustment of the weight and biases to properly predict an output. This value is then compared with the original label, and through the minimization of the Mean Squared Error (MSE), the parameters of the network are updated through backpropagation (Rumelhart et al., 1988). A usual metric to describe the performance of the model is the Root Mean Squared Error (RMSE) shown in eq. 3.

$$\text{RMSE} = \sqrt{\sum_{i=1}^{n} \frac{(y_{real,i} - y_{pred,i})^2}{n}} \quad \text{(eq. 3)}$$

Similar processes are applied to the training of RNN and LSTM architectures, in which the data is cyclically analyzed to extract temporal relationships. In an RNN, each layer will receive the current input data x_t and the previous hidden state h_{t-1} per timestep. The output $y_{pred,t}$ will depend on the hidden value of the current time step h_t shown in eq. 4 and eq. 5. The graphical representation of the unrolled temporal structure of an RNN is presented in Fig. 3 (b), where each timestep shares weights for the input, hidden and output data through W_x, W_r, W_y and biases in the hidden and output layers b_h, b_y, as follows.

$$h_t = \sigma(W_x \cdot x_t + W_r \cdot h_{t-1} + b_h) \quad \text{(eq. 4)}$$

$$y_t = \sigma(W_y \cdot h_t + b_y) \quad \text{(eq. 5)}$$

LSTM architectures are constructed from the same concept for timeseries analysis. However, this model is equipped with an internal memory cell, which selectively updates depending on the new input values for each timestep (Hochreiter and Schmidhuber, 1997). This allows the model to retain and replicate behavior for longer sequences than RNN models. The Vanilla LSTM is composed of three gates: forget, input and output gates, representing each an individual RNN, shown left to right in Fig. 4 which use logistic sigmoid activation functions to regulate how much information is passed through these gates, between [0,1]. Each cell has three inputs of data for each timestep: from the previous cell state c_{t-1}, previous hidden output h_{t-1} and the new input x_t. As the new data inputs the memory cell, the forget gate (eq. 6) selects which values from the previous state will be erased from the memory cell, while the input gate (eq. 7) selects the information with which the state will be updated with.

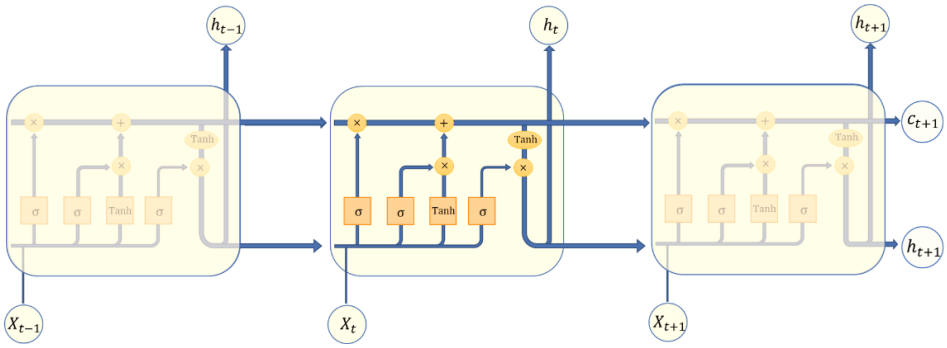

Fig. 4: Basic structure of Vanilla LSTM.

$$f_t = \sigma(W_f x_t + U_f h_{t-1} + b_f) \quad \text{(eq. 6)}$$

$$i_t = \sigma(W_i x_t + U_i h_{t-1} + b_i) \quad \text{(eq. 7)}$$

A new cell state candidate is constructed from the input data (eq. 8). By combining the input and forget gates with the previous state of the cell and the new candidate, the updated cell state is calculated with eq. 9.

$$a_t = tanh(W_c x_t + U_c h_{t-1} + b_c) \quad \text{(eq. 8)}$$

$$c_t = f_t \cdot c_{t-1} + i_t \cdot a_t \quad \text{(eq. 9)}$$

Finally, the output gate defines which information from the cell state will construct the hidden state of the cell through eq. 10 and eq. 11.

$$o_t = \sigma(W_o x_t + U_o h_{t-1} + b_o) \quad \text{(eq. 10)}$$

$$h_t = o_t \cdot tanh(c_t) \quad \text{(eq. 11)}$$

Parametric models, such as DNN, RNN and LSTM, are defined by trainable parameters called hyperparameters. An adequate choice for these values significantly impacts the performance of the models. Depending on the nature of the data and the required task, the number of layers and units per layers, activation functions, learning

rates, optimizers, batch size and training epochs must be selected. An important aspect of these hyperparameters is impact that present on the abstract representation of the data within the latent space of the model. From the learned latent space, the performance of the model will depend on how similar or dissimilar the new input data is compared to the training set used to construct that latent space. For instance, for complex data mapping, such as physical phenomena, it has been reported that architectures with more layers and less units per layer are preferred (Graves et al., 2013; Levine et al., 2017). Adam and RMSProp are assessed as optimizers (Kingma and Ba, 2014; Tijmen and Geoffrey E., 2012), while the hyperbolic tangent (eq. 12) and the Rectified Linear Units functions (eq. 13) are used as activation functions.

$$tanh(x) = \frac{2}{1+e^{-2x}} - 1 \qquad \text{(eq. 12)}$$

$$ReLU(x) = \begin{cases} 0 \; for \; x < 0 \\ x \; for \; x \geq 0 \end{cases} \qquad \text{(eq. 13)}$$

The ANN, RNN and LSTM models were tested under different conditions regarding the length of the temperature sequence they were required to learn and replicate. One, three and seven days of continuous previous data sequences and their effect on the performance of the models was tested. The size of the datasets for each sequence length is detailed in Table 4. Models were compared with the RMSE metric, as well as the relative prediction error for single temperature predictions. Furthermore, their ability to predict longer sequences was analyzed.

Tab. 4: Number of samples per time-window length.

Dataset	N° Previous Days	Time-window Size	Train Set	Validation Set	Test Set
Solar	1	240	5836	1460	1824
Collector	3	720	17510	4378	5472
Outlet T°	7	1680	23654	5919	7393

4. Results and Discussion

This section presents the results obtained when assessing the DL architectures applied for temperature prediction and anomaly detection. Initially, various potential candidate DL models are trained and tested with data in nominal operational conditions. From this assessment, one trained model is selected for anomaly detection purposes. This selected model is tested with fault-free and fault-induced data and the prediction errors will be compared. From this, a threshold is determined to separate and classify the health state of the system between nominal and anomalous conditions.

Simulated data from the TRSNSYS model is processed through sliding windows, generating the sequences which the DL models are trained. The predictions of the solar collector field's outlet temperature considered the following variables of the system as inputs: ambient temperature, inlet temperature of solar field, control signal of solar pumps and inlet temperature of the heat exchanger connected to the pre-heating tanks. Datasets are normalized and separated into training (20%), validation (16%) and test sets (64%).

The following hyperparameters were assessed for DNN, RNN and LSTM architectures: number of units and layers, activation functions, optimizer, training epochs; and batch sizes, as seen in Tab. 5. These different configurations were trained, validated and tested with each independent dataset; and their performance is compared, seeking for accurate and precise predictions.

Tab. 5: Tested hyperparameters and architectures.

Model	DNN, RNN, LSTM
Data Length	1-3-7 Days
Number of layers	1-2-3
Number of RNN units	16, 32, 64, 128, 256
Number of MLP units	128, 256, 512, 1024
Activation Function	Tanh, ReLU
Optimizer	Adam, RMSProp
Epochs	50, 75, 100, 150, 200
Batch Size	32, 64, 128

4.1 Temperature Prediction

The criteria used to assess the performance of trained models is low RMSE values and low variance for both single time-step ahead value and sequence predictions obtained over the test sets. The best results for single value predictions were obtained with an RNN-based model, but LSTM achieved more precise predictions for temperatures sequences; and both outperform ANN architectures.

In Table 6, the obtained test errors and their related statistical metrics are presented for different configurations, in which those models with a variance below 1°C have been highlighted in bold font. Here, the effect of the prior data sequence's length used to train the model can be visualized as follows: for DNN and RNN, the use of the whole previous day as input data is enough to predict the following timesteps' output accurately. However, LSTM requires longer sequences to reach comparable results. The improvement of the LSTM's performance with a three day-length temporal matrix reaches an RMSE below 1°C, but the difference is not significant to when a seven-day sequence is analyzed.

Tab. 6: Test errors and statistical metrics for trained models.

Model	Num. Days	Units	Test Error	Variance	R2	Explained Variance
DNN	1	64-32	1.74	2.910	0.986	0.986
RNN	1	64	1.68	2.460	0.987	0.988
DRNN	1	64-32	1.28	1.221	0.993	0.993
LSTM	1	64	2.5	3.410	0.982	0.984
DNN-1	3	64-32	1.43	1.587	0.988	0.991
DNN-2	3	64-32-16	1.29	1.502	0.990	0.991
DNN-3	3	128-64	1.66	2.425	0.984	0.986
DRNN-1	3	64-32	0.92	1.516	0.991	0.991
DRNN-2	3	64-32-16	0.89	0.619	0.996	0.996
DLSTM-1	3	64-32	1.42	0.618	0.996	0.996
DLSTM-2	3	128-64	1.47	0.520	0.997	0.997
DLSTM-3	3	128-64-32	1.66	0.898	0.993	0.995
DNN	7	64-32-16	1.26	1.550	0.991	0.991
DRNN	7	64-32	0.94	0.644	0.996	0.996
DLSTM	7	64-32	1.38	1.510	0.991	0.991

The performance of the three top-performing models under similar conditions was compared in Table 7 for MAE and RMSE scores. While the DNN model is consistently outperformed by the RNN and LSTM models, the latter yields a lower variance for more than half of the samples tested. This result may explain the reason for more extensive use of DNN models compared to more complex models which require significant efforts to select adequate hyperparameters and training conditions, as well as longer training times. However, the results yielded by the LSTM model suggest that sequence predictions can effectively benefit from the use of this architecture, given the availability of long enough previous data sequences.

Tab. 7: Sequence reconstruction error trained with a three-day time-window.

	DNN-2			*DRNN-2*			*DLSTM-2*		
Sample	**Mean**	**STD**	**RMSE**	**Mean**	**STD**	**RMSE**	**Mean**	**STD**	**RMSE**
1	3.39	5.35	6.33	2.11	4.28	5.46	0.57	3.99	4.03
2	2.55	0.92	2.71	1.66	0.94	1.77	0.46	0.49	0.67
3	0.74	0.50	0.89	-0.10	0.59	2.55	-0.75	0.36	0.83
4	0.90	0.31	0.95	0.28	1.53	1.29	0.08	0.43	0.43
5	-0.49	0.67	0.83	-0.13	0.40	0.04	0.03	0.55	0.55
6	0.62	1.57	1.68	-1.36	2.59	2.89	1.09	2.13	2.39
7	0.86	0.40	0.95	0.49	0.69	0.65	1.40	0.36	1.45
8	1.40	0.73	1.58	-0.32	1.06	0.30	0.12	0.88	0.89
9	1.17	0.56	1.29	0.16	0.41	0.26	0.80	0.43	0.91
10	0.62	0.69	0.92	-0.20	0.36	0.60	0.17	0.50	0.53
Average	**1.18**	**1.17**	**1.81**	**0.16**	**1.28**	**1.58**	**0.40**	**1.01**	**1.27**
STD			**1.60**			**1.68**			**1.07**
MAE	**1.27**			**0.41**			**0.55**		

The best performing model obtained was the two layered LSTM with an output hidden layer, obtaining a mean RMSE of 1.27°C, MAE of 0.55°C with a mean standard deviation of 1.01 over ten random sequence samples during operating hours of the solar field. The selected architecture is presented in Table 8.

Tab. 8: Selected Deep Learning model.

Hyperparameter	Value
Architecture	LSTM
Units & layers	128-64
Activation function	Tanh
Optimizer	RMSProp
Learning rate	10^{-3}
Batch size	64
Epochs	150
Length of time-window	3 days
MLP hidden units	512

4.2 Anomaly Detection

The generated healthy and anomalous sequences were fed to the LSTM model and then the prediction errors were analyzed. By training the algorithms with fault-free data, it is expected to perform worse when presenting them with fault-induced temperatures. Fault-induced data profiles are generated by the TRNSYS deck: an anomalous water-draw profile and the reduction of the solar collector's efficiency are studied in detail for samples extracted at different meteorological conditions.

The discrepancy between predicted and observed values is then classified as anomalous behavior by defining a proper threshold. This threshold depends on the performance of the trained model with each new time series presented and is not dependent of a manually selected value. The response of the system to the induced fault is recorded for two hours, in which at least have an hour is needed to correctly identify unexpected behavior. This limits the real-time implementation of the model, which needs to be assessed with each system's thermal inertia.

The proposed method to identify anomalies consists of using the trained model's prediction values variance as a threshold to classify health states of the system. This yields accurate results for the water-draw anomalous behavior, in which the system's temperatures rise over expected trends. This scenario is recognized with a mean accuracy of 86% and precision, recall, F-1 score and specificity of 85%. Case 1 and 3 present favorable results, however, Case 2, occurring during mid-winter, present additional difficulty to recognize anomalous behavior.

Fig. 5 shows how the anomalous profile generates higher prediction errors, indicating that the model's latent representation of the healthy data is different enough to be recognized as an anomaly. As the LSTM model uses previous predictions to construct the whole temperature sequence, it is expected that the reconstruction errors increase when in predicting a larger horizon. However, as the prediction error increases during the 20 future timesteps for the anomalous profiles, the healthy reconstruction errors are consistently lower. Additionally, the anomalous predictions tend to constantly overestimate the anomalous-induced temperatures. That effect allows defining a separation between healthy and anomalous data by selecting a threshold based on the variance of the reconstruction errors. Classification metrics, such as precision, recall, accuracy, F1 and specificity scores are presented for this scenario in Tab. ***9***.

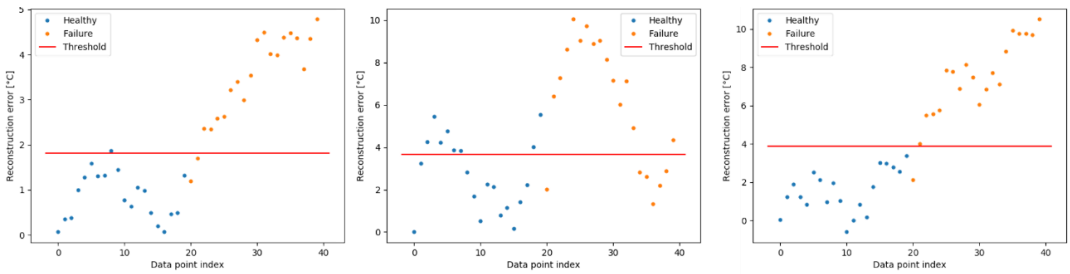

Fig. 5: Anomalous water-draw detection threshold.

Tab. 9: Anomaly detection classification metrics for overheating scenario.

Precision	Recall	Accuracy	F1	Specificity
0.85	0.85	0.85	0.85	0.85

Regarding the collector efficiency anomaly, the reconstruction errors sequence is shown in Fig. 6, which presents higher prediction errors for the healthy input data than the anomalous profile, overestimating the sequence of temperatures. Since the threshold is based on the variance of the prediction's errors, as discussed above, the detection logic is inversed as the anomaly corresponds to lower temperatures than expected. In that context, any datapoint which is within the dispersion of the anomalous predictions is recognized as an anomalous state. The higher number of false positives reduces the overall confidence of the detector, indicating that heat underproduction is harder to capture and recognize as an anomaly from the characteristics learned by the model. From the perspective of the thermal model, the effect of the lower radiation absorbed is reduced by the constant heat influx from the heat-recovery chiller and the returning flow from the heat pump circuit. This may also reflect that the representation of the data in the latent space of the LSTM-based model requires other inputs which can indicate the presence of low anomalous temperatures in the system. This result is reflected on the lower scores obtained for this scenario, presented in Tab. ***10***.

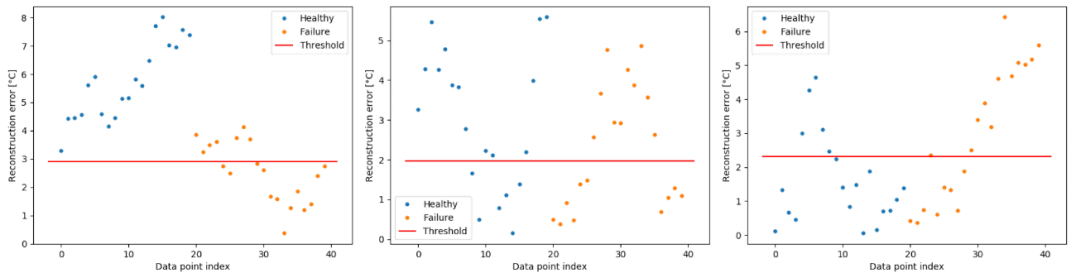

Fig. 6: Anomalous collector behavior detection threshold.

Tab. 10: Anomaly detection classification metrics for heat underproduction scenario.

Precision	Recall	Accuracy	F1	Specificity
0.82	0.63	0.68	0.71	0.76

A significant difficulty in detecting anomalies is found when the temperatures are lowered. This is due to the operation of the auxiliary sources which maintain a regular temperature throughout, even though the solar field's heat input is insignificant. Both results indicate the need to integrate temporal criteria into the detection algorithm. Additionally, the constant input from the auxiliary sources and the restrictions of the control system limit the number of operating hours of the system. This may unnecessarily induce bias on the results, toward lower temperatures and thus reducing the model's performance toward lower heat input scenarios.

5. Conclusions

The present work aims to assess the application of DL algorithms for performance prediction in SHW systems, as well as exploring its usefulness as an anomaly detection tool. The system analyzed is based on a SWH installation built in TRNSYS, which allows generating large amounts of synthetic data. This approach results useful since it allows to adapt the model to the physical configuration of the system, disregarding the commonly high uncertainties related to the sensors used in thermal systems.

In addition, different configurations of frequently used architectures such as DNN, and specialized algorithms for timeseries analysis as RNN and LSTM, were trained as potential candidates for temperature prediction and their performance compared. Low RMSE and MAE values were obtained, suggesting that a successful implementation is possible. Among the different architectures analyzed, the trained LSTM model yielded more accurate predictions than DNN model; and more precise values than RNN for temperature sequence predictions.

However, further work is required when analyzing non-favorable operating scenarios of the solar field. A crucial step to develop a robust fault detection algorithm is to obtain a reliable latent representation of the data,

considering an implementation of a real-time monitoring and prognosis of the SHW system. For this, other pre-processing techniques and architectures will be explored.

The limitation of this framework is that the synthetic data was generated with a simulation platform. TRNSYS is a validated physics-based model which allows the incorporation of the real SHW installations technical specifications and quality meteorological measurement. Yet, the simplifications established in the simulation program, such as the restrictions on the control system and the ideal conditions of the auxiliary heat inputs, reduce the number of hours in which the solar field is operational.

The results show the strengths and shortcomings of an initial approach for anomaly detection in a SHW system. The use of synthetic data allowed to isolate and study specific behaviors and anomalies without temporal limitations and measurement uncertainties. However, data recollection is a vital step for developing DL-based algorithms and the use of synthetic data also allows time-saving strategies to explore different alternatives before actual implementation in a real system. That approach is highly useful for conducting field assessments when the historical information is not available; however, its representativity of the thermal system is limited for anomalous scenarios.

While further tuning of the model's hyperparameters is required, specialized architectures for time-series analysis, such as RNN and LSTM have proven to capture and replicate temperature sequences better than DNN-based models. Finally, other data-based metrics can be explored for anomaly and fault detection in systems by quantifying the uncertainty of the experimental measurements, the simulation's results, and the model's predictions.

6. Acknowledgments

The authors appreciate the financial support from CONICYT/FONDAP 15110019 "Solar Energy Research Center" SERC-Chile.

7. References

Ayompe, L.M., Duffy, A., McCormack, S.J., Conlon, M., 2011. Validated TRNSYS model for forced circulation solar water heating systems with flat plate and heat pipe evacuated tube collectors. Appl. Therm. Eng. 31, 1536–1542. https://doi.org/10.1016/j.applthermaleng.2011.01.046

Burch, J., Christensen, C., 2007. Towards Development of an Algorithm for Mains Water Temperature. InterSolar 2007 Conf. 5–10.

Correa-Jullian, C., Cardemil, J.M., Droguett, E.L., Behzad, M., 2019. Assessment of Deep Learning Techniques for Prognosis of Solar Thermal Systems. Renew. Energy 145, 2178–2191. https://doi.org/10.1016/j.renene.2019.07.100

de Keizer, A.C., Vajen, K., Jordan, U., 2011. Review of long-term fault detection approaches in solar thermal systems. Sol. Energy 85, 1430–1439. https://doi.org/10.1016/j.solener.2011.03.025

de Keizer, C., Kuethe, S., Jordan, U., Vajen, K., 2013. Simulation-based long-term fault detection for solar thermal systems. Sol. Energy 93, 109–120. https://doi.org/10.1016/j.solener.2013.03.023

Ghritlahre, H.K., Prasad, R.K., 2018. Application of ANN technique to predict the performance of solar collector systems - A review. Renew. Sustain. Energy Rev. 84, 75–88. https://doi.org/10.1016/j.rser.2018.01.001

Graves, A., Mohamed, A.R., Hinton, G., 2013. Speech recognition with deep recurrent neural networks, in: ICASSP, IEEE International Conference on Acoustics, Speech and Signal Processing - Proceedings. pp. 6645–6649. https://doi.org/10.1109/ICASSP.2013.6638947

Hochreiter, S., Schmidhuber, J., 1997. Long Short-Term Memory. Neural Comput. 9, 1735–1780. https://doi.org/10.1162/neco.1997.9.8.1735

IRENA, 2018. Opportunities to accelerate national energy transitions through advanced deployment of renewables.

Janssens, O., Van de Walle, R., Van Hoecke, S., Loccufier, M., Verstockt, S., Vervisch, B., Stockman, K., Slavkovikj, V., 2016. Convolutional Neural Network Based Fault Detection for Rotating Machinery. J. Sound Vib. https://doi.org/10.1016/j.jsv.2016.05.027

Kalogirou, S., Lalot, S., Florides, G., Desmet, B., 2008. Development of a neural network-based fault diagnostic system for solar thermal applications. Sol. Energy 82, 164–172. https://doi.org/10.1016/j.solener.2007.06.010

Kalogirou, S.A., Agathokleous, R., Barone, G., Buonomano, A., Forzano, C., Palombo, A., 2019. Development and validation of a new TRNSYS Type for thermosiphon flat-plate solar thermal collectors: energy and economic optimization for hot water production in different climates. Renew. Energy 136, 632–644. https://doi.org/10.1016/j.renene.2018.12.086

Kingma, D.P., Ba, J., 2014. Adam: A Method for Stochastic Optimization. AIP Conf. Proc. 1631, 58–62. https://doi.org/10.1063/1.4902458

Klein, S.A., 2018. TRNSYS: A transient systems simulation program v.18.00.0019.

Leva, S., Dolara, A., Grimaccia, F., Mussetta, M., Ogliari, E., 2017. Analysis and validation of 24 hours ahead neural network forecasting of photovoltaic output power. Math. Comput. Simul. 131, 88–100. https://doi.org/10.1016/j.matcom.2015.05.010

Levine, Y., Sharir, O., Ziv, A., Shashua, A., 2017. On the Long-Term Memory of Deep Recurrent Networks. Iclr2018 1–23.

Lipton, Z.C., Berkowitz, J., Elkan, C., 2015. A Critical Review of Recurrent Neural Networks for Sequence Learning. Proc. ACM Int. Conf. Multimed. - MM '14 675–678. https://doi.org/10.1145/2647868.2654889

Lui, Y., Zhao, G., Peng, X., Hu, C., 2017. Lithium-ion battery remaining useful life prediction with long short-term memory recurrent neural network. Annu. Conf. Progn. Heal. Manag. Soc. 1–7.

Niu, G., 2017. Data-Driven Technology for Engineering Systems Health Management. Springer Singapore, Singapore. https://doi.org/10.1007/978-981-10-2032-2

Ruiz, E., Martínez, P.J., 2010. Analysis of an open-air swimming pool solar heating system by using an experimentally validated TRNSYS model. Sol. Energy 84, 116–123. https://doi.org/10.1016/j.solener.2009.10.015

Rumelhart, D.E., Hinton, G.E., Williams, R.J., 1988. Learning Internal Representations by Error Propagation, in: Readings in Cognitive Science. Elsevier, pp. 399–421. https://doi.org/10.1016/B978-1-4832-1446-7.50035-2

Souliotis, M., Kalogirou, S., Tripanagnostopoulos, Y., 2009. Modelling of an ICS solar water heater using artificial neural networks and TRNSYS. Renew. Energy 34, 1333–1339. https://doi.org/10.1016/J.RENENE.2008.09.007

Srivastava, S., Lessmann, S., 2018. A comparative study of LSTM neural networks in forecasting day-ahead global horizontal irradiance with satellite data. Sol. Energy 162, 232–247. https://doi.org/10.1016/j.solener.2018.01.005

Tijmen, T., Geoffrey E., H., 2012. Lecture 6.5- RMSprop: Divide the gradient by a running average of its recent magnitude [WWW Document]. COURSERA Neural Netw Mach Learn 42.